Chemical Science

ROYAL SOCIETY OF CHEMISTRY

EDGE ARTICLE

View Article Online
View Journal | View Issue

Cite this: *Chem. Sci.*, 2025, **16**, 9802

All publication charges for this article have been paid for by the Royal Society of Chemistry

Achieving dual emission of thermally activated delayed fluorescence and ultralong room-temperature phosphorescence by controlling excited state dynamics through metal coordination†

Xian-Bao Cai,[ab] Dong Liang,[a] Deng-Chao Zhang,[c] Ji-Hui Jia,[c] Xiao-Yuan Wu[a] and Can-Zhong Lu*[abd]

Received 22nd January 2025
Accepted 18th April 2025

DOI: 10.1039/d5sc00555h

rsc.li/chemical-science

Controlling excited-state dynamics is crucial for achieving dual emissions of ultralong room-temperature phosphorescence (URTP) and thermally activated delayed fluorescence (TADF), but remains challenging in the exploration of transition-metal compounds. Herein, we propose a new strategy to develop highly efficient TADF and URTP dual-emission materials by modulating URTP organic molecules through metal ion coordination. Specifically, Ag^+ ions narrow the singlet-triplet energy gap (ΔE_{ST}) and enhance spin–orbit coupling (SOC), thereby accelerating intersystem crossing (ISC) and facilitating reverse intersystem crossing (RISC). The Ag^+ ions also balance radiative transitions and RISC processes of the T_1 state. Consequently, coordinating the URTP molecule Phen-Tpa with Ag^+ ions results in an Ag(I) complex that exhibits efficient ligand-centered TADF and URTP dual emissions in MeOBP films, with a quantum yield of 85%, an afterglow duration of 6 seconds, and a record long emission lifetime of 575.7 ms. Moreover, Phen-Tpa can be used to fabricate organic white light-emitting diodes (LEDs), while both Phen-Tpa and the Ag(I) complex offer high-security anti-counterfeiting capabilities. These results deepen the understanding of how metal fragment coordination influences luminescence mechanisms and provide a new approach for achieving dual emissions with coexisting TADF and URTP in transition-metal compounds.

Introduction

Luminescent materials exhibiting thermally activated delayed fluorescence (TADF) and room-temperature phosphorescence (RTP) have gained significant attention due to their promising applications in organic light-emitting diodes (OLEDs), sensors, bio-imaging, and anti-counterfeiting technologies.[1–9] Among RTP materials, ultralong room-temperature phosphorescence (URTP) stands out due to its exceptionally extended emission lifetimes, making it particularly suitable for persistent luminescence applications. Despite substantial advancements in the development of high-performance materials, most of them exhibit only a single type of emission. Materials that display both TADF and RTP dual-emission characteristics are highly desirable for their potential for improved performance and significant advantages in medical resolution and anti-counterfeiting encryption.[10–13] However, achieving dual TADF and URTP emissions in a single material is especially difficult due to the competition between radiative transitions and RISC processes of triplet excitons. This intricate interplay demands precise control over the dynamics of excited states. The rates of RISC and ISC can be described by Fermi's golden rule:[14,15]

$$k_{ISC(RISC)} \propto \langle {}^1\Psi|\hat{H}_{SO}|{}^3\Psi\rangle/\exp(\Delta E_{ST}{}^2)$$

where ${}^1\Psi$ and ${}^3\Psi$ represent the wavefunctions of singlet and triplet states, $\hat{H}_{SO}$ is the SOC Hamiltonian, and ΔE_{ST} is the energy gap between the singlet and triplet states. This equation underscores the critical roles of ΔE_{ST} and SOC in determining RISC and ISC rates, which directly influence TADF and URTP emissions. For TADF emitters, design strategies often focus on donor–acceptor (D–A) compounds, where the spatial separation

[a]*CAS Key Laboratory of Design and Assembly of Functional Nanostructures, Fujian Provincial Key Laboratory of Nanomaterials, Fujian Institute of Research on the Structure of Matter, Chinese Academy of Sciences, Fuzhou, Fujian 350002, China. E-mail: czlu@fjirsm.ac.cn*

[b]*College of Chemistry, Fuzhou University, Fuzhou, 350116, P. R. China*

[c]*School of Materials Science and Engineering, Fujian University of Technology, Fuzhou, Fujian, 350118, P. R. China*

[d]*Fujian College, University of Chinese Academy of Sciences, Fuzhou, Fujian 350002, China*

† Electronic supplementary information (ESI) available. CCDC 2414838 and 2414839. For ESI and crystallographic data in CIF or other electronic format see DOI: https://doi.org/10.1039/d5sc00555h

of the highest occupied molecular orbital (HOMO) and the lowest unoccupied molecular orbital (LUMO) effectively reduces the ΔE_{ST}, facilitating the conversion of triplet excitons into luminescent singlet excitons *via* RISC.[16–24] In contrast, designing URTP emitters requires meeting distinct criteria: efficient ISC to generate triplet excitons, typically achieved through the incorporation of heavy atoms or heteroatoms containing *n*-electrons; a rigid environment to suppress non-radiative decay of triplet excitons; a slow phosphorescence decay rate (k_p) to ensure a long phosphorescence lifetime.[25–30] Balancing the distinct requirements for achieving dual-emission systems capable of both TADF and URTP presents a significant challenge, largely due to the limited understanding of how to effectively control excited-state dynamics.

TADF and URTP phenomena have also been reported in certain Ag(I) complexes.[31–35] In 2019, Yersin and co-workers designed an Ag(I) material that exhibits intense phosphorescence with an unprecedentedly long lifetime of $\tau = 110$ ms.[36] In this Ag(I) complex, the lowest triplet state frequently features a ligand-centered (LC) character due to relatively high ionization potential of Ag(I) with low-lying d-orbitals. This LC property also contributes to ligand-centered fluorescence and long-lived phosphorescence in many Ag(I) complexes.[37,38] Consequently, the development of Ag(I) TADF compounds has been significantly hindered. Therefore, Lu and co-workers have focused on the ligand-centered nature of silver compounds as a novel approach to designing TADF, referred to as coordination-induced TADF.[39,40] In these materials, the HOMO and LUMO are mainly distributed on the donor and acceptor (D–A) moieties of the ligand, and the corresponding excited states (S_1 and T_1) typically exhibit intra-ligand charge transfer (ILCT) characteristics. The coordination of silver ions significantly reduces ΔE_{ST} and enhances SOC between S_1 and T_1, thereby facilitating RISC and enabling the generation of TADF, which highlights the crucial role of silver ions in regulating excited-state dynamics. It is widely accepted that silver ions play a crucial role in regulating emission mechanisms and achieving TADF and URTP emissions. However, their specific role in modulating dual-emission systems that combine TADF and URTP remains largely unexplored. Therefore, investigating the influence of metal ions on controlling these dual-emission behaviors is of great significance. Such dual-emission materials are not only important for advancing our understanding of new luminescence mechanisms but also hold significant potential for enabling advanced applications.[26]

In this paper, dual TADF and URTP emissions were successfully achieved through metal coordination. We synthesized the previously reported pure organic D–A-type phosphorescent molecule,[41] 4,4′-(1,10-phenanthroline-3,8-diyl)bis(*N*,*N*-diphenylaniline) (Phen-Tpa), in which the triphenylamine (Tpa) groups act as electron donors and the phenanthroline moiety (Phen) acts as an electron acceptor. The photophysical properties of the ligands in MeOBP films were investigated, revealing white emission with CIE (*x*, *y*) coordinates of (0.31, 0.32) and yellow afterglow photoluminescence (PL), achieving a total quantum yield of 99% and a phosphorescence quantum yield of up to 37.2%. It also displays a long RTP lifetime of 781.6 ms. With the Phen-Tpa and phosphine ligands (4,5-bis(diphenylphosphino)-9,9-dimethylxanthene (Xantphos)), a green- and yellow afterglow-emitting Ag(I) complex was designed, exhibiting ligand-centered TADF and URTP dual emission pathways that coexist in the films, with a high quantum yield of 85% and a long lifetime of 575.7 ms at room temperature. In addition, the intriguing luminescent properties of Phen-Tpa and its silver complex make them promising candidates for white LED devices and anti-counterfeiting applications. To the best of our knowledge, this compound is the first reported Ag(I) molecule that simultaneously exhibits both TADF and URTP properties, along with the longest emission lifetime. Our findings not only provide a new strategy for designing Ag(I) compounds with dual TADF and URTP emission capabilities and long afterglow properties, but also offer deeper insights into how metal fragment coordination influences luminescence mechanisms, expanding the potential for high-performance application.

Results and discussion

The Phen-Tpa ligand was readily synthesized in a single step *via* Suzuki coupling (Scheme S1†). Complex **1** was obtained by reacting the Phen-Tpa ligand, $[Ag(CH_3CN)_4]BF_4$, and the phosphine ligand 4,5-bis(diphenylphosphino)-9,9-dimethylxanthene (Xantphos) in a CH_2Cl_2 solution. The Ag(I) complex was purified by recrystallization through the slow diffusion of toluene into a CH_2Cl_2 solution. Both Phen-Tpa and complex **1** were characterized by ^{1}H NMR, ^{13}C NMR, and elemental analyses, with the corresponding spectra provided in the ESI.† Complex **1** is air-stable in the solid state. Thermogravimetric analysis (TGA) indicated that Phen-Tpa and complex **1** exhibit excellent thermal stability, with decomposition temperatures of 520 °C and 414 °C, respectively.

The chemical and X-ray structures of the free Phen-Tpa ligand and its silver complex are shown in Fig. 1a; selected crystallographic data are listed in Table S1.† As shown in Fig. 1a, the Ag(I) cation chelated with the free ligand Phen-Tpa and the phosphorus ligand Xantphos to form twisted tetrahedral structures. The Ag–N distances are 2.317(15) and 2.374(18) Å, and the Ag–P distances are 2.513(6) and 2.389(6) Å. These distances are in the normal range. The dihedral angle between P–Ag–P and N–Ag–N in complex **1** is 86.2(6)°. The dihedral angles between the donor triphenylamine moieties and the acceptor phenanthroline are 19.504(19)° and 47.071(17)° for the Phen-Tpa ligand and 33.298(25)° and 46.754(10)° for complex **1** (Fig. S1†). Compared to the free ligand Phen-Tpa, complex **1** exhibits a larger torsion angle between the donor and acceptor moieties, which leads to a reduced ΔE_{ST} and improved TADF performance.

To investigate the influence of metal coordination on photophysical properties, the UV-vis absorption and emission spectra of the Phen-Tpa ligand and complex **1** were measured. The photophysical parameters are listed in Table 1. The energy levels of these compounds calculated from their electrochemical and photophysical data are summarized in Table 2. Fig. 1b shows the UV-vis spectra of Phen-Tpa and complex **1** in

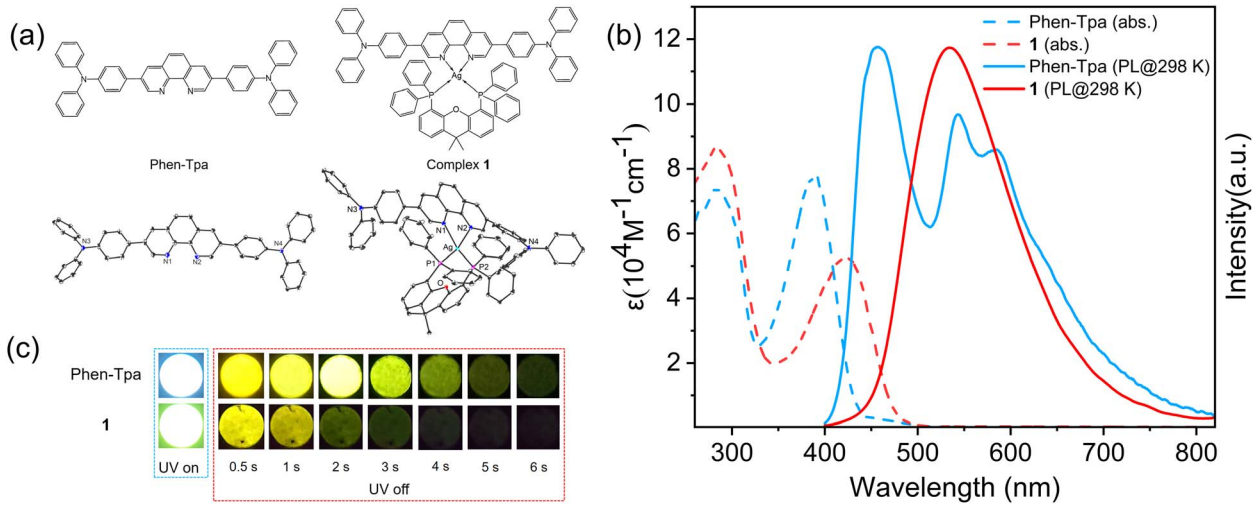

Fig. 1 (a) X-ray and chemical structures of free ligand Phen-Tpa and complex **1**. The hydrogen atoms, anions and solvent molecules are omitted for clarity. (b) Absorption spectra of complex **1** and Phen-Tpa in CH_2Cl_2 (2×10^{-5} M) solution and PL spectra at 298 K for doping in 4-methoxybenzophenone (MeOBP) films (0.05 wt%). (c) Photographs of complex **1** and Phen-Tpa doped in MeOBP films (0.05 wt%) under a 365 nm UV lamp and after ceasing UV excitation.

Table 1 Photophysical parameters of Phen-Tpa and complex **1** doped into MeOBP films (0.05 wt%) in air

	298 K										77 K	
Compound	λ_{max} (nm)	Φ_{PL}[a] (%)	Φ_{DF}[b] (%)	Φ_P[b] (%)	τ_F (ns)	τ_{TADF} (ms)	τ_P (ms)	k_{ISC}[c] (108 s^{-1})	k_{RISC}[c] (s^{-1})	k_p (s^{-1})	λ_{max} (nm)	τ (ms)
Phen-Tpa	456, 544, and 584	99	—	37.2	2.0	—	781.6	1.86	—	1.28	542	1129
1	532	85	40.9	34.8	2.2	13.8	575.7	4.0	358.7	1.74	550	737

[a] Measured in the film with excitation wavelengths of 450, 400 nm for **1** and Phen-Tpa. [b] The phosphorescence (Φ_P) portions [%] for Phen-Tpa estimated from the quantum yields of the emission band between 512 and 820 nm. For complex **1**, the delayed fluorescence (Φ_{DF}) and phosphorescence (Φ_P) portions [%] were estimated from transient PL decay curves and Φ_{PL}. [c] Calculated ISC rate constant (k_{ISC}) and RISC rate constant (k_{RISC}) using exciton lifetime and Φ_{PL} values.

CH_2Cl_2 solution. The absorption spectra of the free ligand Phen-Tpa and complex **1** exhibit intense absorption bands between 260–450 nm and 260–475 nm, respectively, assigned to the $\pi \rightarrow \pi^*$ transitions within the Phen-Tpa and phosphine ligands. In addition, the broad absorptions at around 450 to 500 nm for Phen-Tpa and 475 to 520 nm for complex **1** are attributed to the charge transfer from the donor to the acceptor moieties. The absorption spectrum of complex **1** is clearly red-shifted compared to that of the Phen-Tpa ligand, indicating a slightly smaller HOMO–LUMO gap, consistent with the DFT and TD-DFT calculation results. The optical energy gaps (E_g) estimated from the absorption edges are 2.88 eV and 2.65 eV for the Phen-Tpa ligand and complex **1**, respectively. To further investigate the photophysical properties of Phen-Tpa and complex **1**, organic films were fabricated by doping both compounds at a 0.05 wt% concentration in 4-methoxybenzophenone matrices using the melt-casting technique, following a previously reported procedure.[42–44] A low dopant concentration was used to prevent the quenching caused by high concentrations of triplet excitons. As shown in Fig. 1c, both Phen-Tpa and complex **1** emit in the organic films, with afterglow durations of 6 to 7 seconds. Fig. 1b shows the steady-state

Table 2 Energy levels and gaps of Phen-Tpa and complex **1**

Compound	E_g[a] eV	HOMO[b] eV	LUMO[c] eV	^{1}CT[d] eV	^{3}LE[e] eV	ΔE_{ST}[f](exp.) eV
Phen-Tpa	2.88	−5.33	−2.45	3.01	2.48	0.53
1	2.65	−5.41	−2.76	2.73	2.53	0.20

[a] Estimated from the onset wavelengths of the absorption spectra measured in CH_2Cl_2 solution. [b] Calculated from the oxidation potentials of cyclic voltammetry measured in CH_2Cl_2 solution. [c] Calculated from the HOMO energy levels and ΔE_g. [d] Estimated from the onset prompt fluorescence for **1** and Phen-Tpa. [e] Estimated from the onset wavelengths of the 298 K emission spectra (delayed 150 ms for **1** and delayed 68.3 ms for Phen-Tpa). [f] $\Delta E_{ST} = {}^1CT - {}^3LE$.

PL spectra of Phen-Tpa and complex **1** in air. The structured spectrum of Phen-Tpa indicates that the excited state has local excitation (LE) characteristics. The free Phen-Tpa ligand exhibits white emission with CIE (x, y) coordinates of (0.31, 0.32) and displays a yellow afterglow PL in MeOBP films at room temperature, with a high quantum yield of 99%. The transient PL decay spectra of Phen-Tpa at 298 K show a prompt fluorescence lifetime of 2 ns for the S_1 excited state, followed by long-lived phosphorescence with a lifetime of 781.6 ms (Fig. S7† and 2a). Time-resolved PL spectra (Fig. 2c) of the Phen-Tpa ligand show a redshift of the PL maximum from 456 to 544 nm after a delay of 5 ns and exhibit a strong vibrational shape after a delay of 68.3 ms at room temperature, indicating that the delayed emissions are not TADF. The different emission profiles at various delayed times demonstrate that the ligand has two components, ascribed to prompt fluorescence and ultralong RTP. Based on the above analysis, the emission band from 512 to 820 nm, primarily attributed to phosphorescence, exhibits a high quantum yield of 37.2%. The photophysical properties of Phen-Tpa were measured at 77 K to further investigate the nature of its excited states. The steady-state spectrum of Phen-Tpa is shown in Fig. S8a.† It differs from the spectrum at room temperature; the 77 K spectrum shows significantly enhanced phosphorescence, which becomes much stronger than fluorescence. Fig. S8c† shows the time-resolved PL spectrum at 77 K (delayed by 50 ms), which is similar to that at 298 K (delayed by 68.3 ms), with both attributed to the ^{3}LE nature of the T_1 state. From the emission spectra of the free Phen-Tpa ligand in MeOBP films at 298 K, the energy levels of S_1 (3.01 eV) and T_1 (2.48 eV) were estimated (Table 2), with an experimental ΔE_{ST} value of 0.53 eV, which is too large for TADF to occur.

The Ag(I) complex emits greenish and yellow afterglow PL (λ_{max} = 532 nm) in MeOBP films at room temperature and exhibits a high quantum yield of 85%. The PL spectra (Fig. 1b) at 298 K are broad and unstructured, suggesting that the corresponding emissive excited state possesses a charge-transfer character. The transient PL spectra of complex **1** were investigated to clarify the nature of its emissions. As shown in Fig. 2a and S7,† complex **1** displays two-component emission decays: a prompt nanosecond decay and a long-lived decay, with lifetimes of 2.2 ns and 575.7 ms, respectively. The time-resolved PL spectra of complex **1** were measured to further investigate its emission properties. The spectra of complex **1** at different delayed times (10 ns, 2.5 μs, and 3.5 ms) are identical (Fig. 2d), confirming that the delayed emission of complex **1** at room temperature contains TADF. At a delay time of 150 ms, the emission spectrum displays a pronounced red shift and a change in shape, indicating that the emission after 150 ms corresponds to phosphorescence. The delayed fluorescence transient PL spectra of complex **1** were measured (Fig. 2b) and show a long lifetime of 13.8 ms. The different emission profiles at various delayed times demonstrate that complex **1** has three components, attributed to prompt fluorescence, delayed fluorescence, and ultralong RTP. The photophysical properties of complex **1** were also investigated at 77 K. Fig. S8d† shows the time-resolved PL spectrum of complex **1** at 77 K with a delay time of 150 ms, which is consistent with the spectrum observed at 298 K at the same delay time. Both spectra are attributed to the T_1 excited state with LE characteristics. The energy levels of S_1 (2.73 eV) and T_1 (2.53 eV) are estimated (Table 2) from the emission spectra at 298 K, giving an experimental ΔE_{ST} value of 0.20 eV. The smaller ΔE_{ST} compared to the free ligand and the heavy atom effect of Ag^+ ions effectively promote the RISC

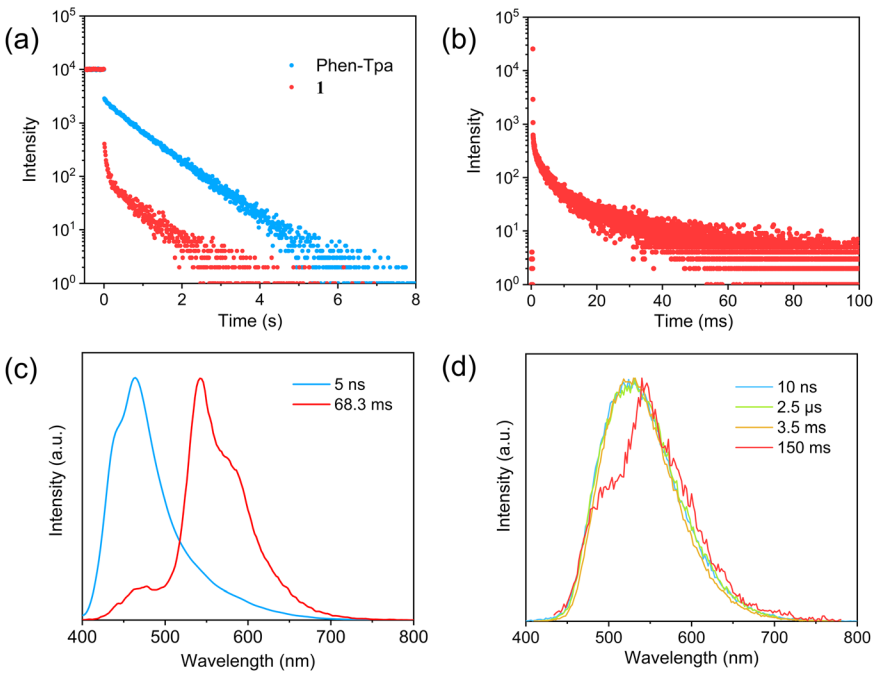

Fig. 2 (a) Transient PL decay spectra of Phen-Tpa and **1**, (b) transient PL decay spectra of the delayed fluorescence of **1**, and (c and d) time-resolved PL spectra of Phen-Tpa and **1** in different time ranges at 298 K doped into MeOBP films (0.05 wt%).

process, enabling the observation of TADF in complex **1**. The k_{RISC} and k_p values calculated from the photophysical properties are 358.7 and 1.74 s^{-1}, respectively, while the k_{ISC} values for Phen-Tpa and complex **1** are 1.86×10^8 and 4×10^8 s^{-1}. In complex **1**, the RISC process is extremely slow, while the ISC process is notably faster compared to the ligand, leading to more efficient accumulation of T_1. The comparable k_{RISC} and k_p values support the simultaneous occurrence of RISC and radiative transitions from T_1, allowing the coexistence of TADF and ultralong RTP dual emissions. The dual emission results from the Ag^+ ions balancing the radiative transition and the RISC processes of the T_1. Additionally, the heavy-atom effect induced by Ag^+ ions accelerates T_1 radiative transitions, resulting in shorter decay times for complex **1** compared to the Phen-Tpa ligand.

To deeply understand the mechanism of the dual emission pathways of TADF and URTP, the molecular and electronic properties of both the ligand and complex **1** were investigated using DFT and TD-DFT calculations. These calculations offered further insights into the emission properties and the corresponding energy levels of the excited states in these compounds. The distributions of the HOMO and LUMO, along with the calculated frontier orbital energies in the optimized S_0 structure, and the singlet (S_1) and triplet (T_1) energy gaps in the optimized S_1 and T_1 structures for Phen-Tpa and complex **1** are shown in Fig. 3a. In both the ligand Phen-Tpa and complex **1**, the HOMO is primarily localized on the triphenylamine donor groups, with a small portion extending to the phenanthroline group, while the LUMO is mainly distributed on the phenanthroline acceptor, with only a minor contribution from the triphenylamine donor. The separation between the HOMO and LUMO in both the free ligand Phen-Tpa and complex **1** is facilitated by the large twisted geometry between the electron-donor (Tpa) and electron-acceptor (Phen) units. The optimized structure of the ligand shows a large gap of 3.73 eV between the HOMO and LUMO. Upon coordination with Ag^+ ions, the energy levels of both the LUMO and HOMO of the ligand are decreased *via* electronic perturbation induced by the Ag^+ ions, whereas the LUMO is stabilized more greatly for its direct connection to the Ag(I) group. The coordination of the Ag^+ ions to the ligand in complex **1** results in a strong stabilization of 2.34 eV for the LUMO, with a smaller change observed in the HOMO energy (1.58 eV), leading to a reduced HOMO–LUMO energy gap of 2.97 eV.

Based on their optimized excited-state structures, the natural transition orbitals (NTOs) of the free Phen-Tpa ligand and complex **1** were analyzed. The SOC calculations were further conducted using the ORCA 5.0 program.[45] The calculation results show that the S_1 and T_1 excited states are predominantly composed of transitions within the Phen-Tpa ligand (Fig. S4†).

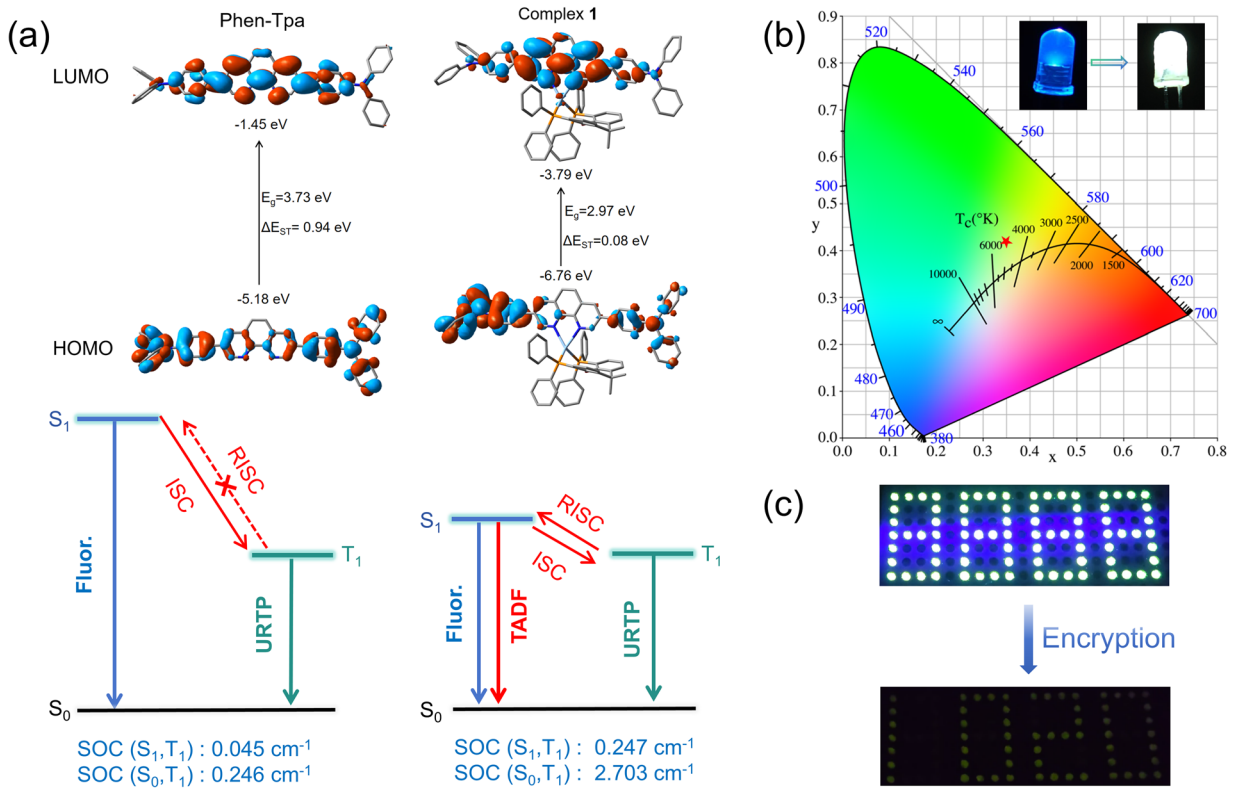

Fig. 3 (a) HOMO and LUMO distribution and calculated frontier orbital energies in the optimized S_0 structure and singlet (S_1) and triplet (T_1) energy gaps in the optimized S_1 and T_1 structures for Phen-Tpa, complex **1** at the PBE0/6-31G*/LANL2DZ levels; PL processes and the SOC constants of the Phen-Tpa ligand and complex **1**. (b) CIE coordinate diagram of a working WLED [inset: the commercially available UV LED light (turning on) and luminescence image of UV LED light coated with a Phen-Tpa film (0.05 wt% in MeOBP) (turning on)]. (c) Encrypted pattern based on Phen-Tpa and **1** powder under 365 nm UV light on and 365 nm UV light off. The longer-lived components consisted of complex **1** (1.5 mg) and Phen-Tpa (0.5 mg) doped into MeOBP (400 mg), while the shorter-lived components included complex **1** (1 mg) doped into MeOBP (400 mg).

The calculated S_1 state is principally composed of the HOMO–LUMO transition (98.56% for complex **1** and 96.24% for Phen-Tpa). NTO analyses indicate that, in complex **1**, the S_1 state is predominantly contributed by the charge transfer transition from the triphenylamine-based donor to the phenanthroline acceptor (81.43%), while in the ligand Phen-Tpa, the S_1 state consists of a combination of charge transfer from the triphenylamine donor to the phenanthroline acceptor (54.46%) and localized excitation (LE) within the phenanthroline acceptor (45.54%). The calculated T_1 state is mainly composed of the HOMO–LUMO transition (68.66% for the ligand and 77.98% for complex **1**). And NTO analyses reveal that T_1 consists of both a charge transfer transition from the triphenylamine-based donor to the phenanthroline-acceptor (53.61% for complex **1** and 19.41% for the Phen-Tpa) and LE inside the phenanthroline-acceptor (43.32% for complex **1** and 80.59% for the Phen-Tpa).

According to the El-Sayed rule,[46] the distinct compositions of the T_1 and S_1 states in complex **1** increase SOC between them, thereby promoting ISC and RISC processes and enhancing TADF. In this case, the Phen-Tpa molecule has a large ΔE_{ST} value of 0.94 eV. The ΔE_{ST} is so large that it is not conducive to the occurence of TADF. Besides, the SOC value of 0.246 cm^{-1} between S_0 and T_1 is significantly higher than the 0.045 cm^{-1} between S_1 and T_1, ensuring a sufficiently fast transition rate from T_1 to S_0 for phosphorescence emission (Fig. 3a). Compared to the ligand Phen-Tpa, complex **1** has a lower calculated ΔE_{ST} of 0.08 eV and significantly increased SOC values of 2.703 cm^{-1} between T_1 and S_0, and 0.247 cm^{-1} between T_1 and S_1. The lower ΔE_{ST} and increased SOC facilitate the occurrence of TADF in complex **1** at room temperature. Meanwhile, the SOC from T_1 to S_0 was large enough, ensuring a relatively rapid transition rate from T_1 to S_0 for phosphorescence emission. From this, the coexistence of TADF and RTP dual emissions is expected to occur in the complex **1**. Based on the theoretical calculations and experimental results, the PL processes of Phen-Tpa and the complex **1** are depicted in Fig. 3a. The Phen-Tpa ligand emits fluorescence and URTP; owing to the large ΔE_{ST} and weak SOC, TADF is not observed. After the coordination of Ag^+ ions, the energy level of the S_1 state is significantly lowered and that of the T_1 state remains essentially unchanged. Therefore, ΔE_{ST} is reduced, and the Ag^+ ions significantly enhance the SOC between the S_1 and T_1 states, thereby accelerating ISC and facilitating RISC. At the same time, the silver ions balance the radiative transition and the RISC process of T_1, resulting in the dual emission of TADF and URTP in complex **1**.

As mentioned above, the free Phen-Tpa ligand shows a white emission. To further authenticate its potential as a promising white-light emitter, we have fabricated a white LED (WLED) with the Phen-Tpa powders (0.05 wt% in MeOBP) covered on a commercial 365 nm UV chip. Then, bright white light emission could be observed when the LED is turned on (Fig. 3b) with CIE (x, y) coordinates of (0.35, 0.42) and a color-rendering index of $R_a = 75$ with a correlated color temperature (CCT) of 4921 K, corresponding to cool white light. Furthermore, the discrepant afterglow lifetime between Phen-Tpa and complex **1** could further improve the security level of anti-counterfeiting. Fig. 3c illustrates an encrypted pattern created using the free ligand Phen-Tpa and complex **1** powder (doped in MeOBP). Under 365 nm excitation, the pattern displays the number "8888", which transitions to "1020" after the light is turned off due to the faster afterglow decay of complex **1** compared to Phen-Tpa. This method enables temporal anti-counterfeiting without the need for sophisticated time-gating technology.

Conclusions

In summary, we demonstrated the coexistence of TADF and URTP dual emission pathways by controlling excited-state dynamics through metal coordination. A D–A type Phen-Tpa ligand was prepared which displays URTP emission. Due to the large ΔE_{ST} and weak SOC of this compound, TADF is not observed. By coordinating with an Ag(I) fragment, complex **1** shows a significant reduction in ΔE_{ST}, along with enhanced SOC between S_1 and T_1 and between T_1 and S_0. Meanwhile, the Ag^+ ions effectively balance the radiative transitions and the RISC processes of the T_1 state. As a result, complex **1** exhibits coexisting ligand-centered TADF and URTP dual emissions in MeOBP films, with a quantum yield of 85%, an afterglow duration of 6 s and a remarkable lifetime of 575.7 ms at room temperature. Furthermore, the remarkable luminescent properties enable the Phen-Tpa ligand to be used in fabricating organic white light-emitting diodes (LEDs), while both the Phen-Tpa ligand and complex **1** provide advanced anti-counterfeiting capabilities. This work provides a feasible pathway for designing Ag(I) compounds with dual-emission capabilities and long afterglow properties, offering deeper insights into how metal fragment coordination influences luminescence mechanisms and expanding the potential for high-performance applications.

Data availability

Detailed experiments, single crystal information, theoretical calculations, and other figures were provided in the ESI file.†

Author contributions

X.-B. Cai proposed the idea, performed the synthesis and characterization of materials, conducted photophysical property measurements, and drafted the manuscript. D. L. contributed to the theoretical calculations and revisions of the manuscript. D.-C. Zhang assisted with electrochemical and UV absorption tests. J.-H. Jia revised the manuscript. X.-Y. Wu supported the crystal analysis, and C.-Z. Lu supervised the project. All authors contributed to the discussion of the results.

Conflicts of interest

There are no conflicts to declare.

Acknowledgements

This work was supported by the National Natural Science Foundation of China (52473202), the Natural Science

Foundation of Fujian Province (2006L2005 and 2021J011073), Fujian Science & Technology Innovation Laboratory for Optoelectronic Information of China (2021ZR132 and 2021ZZ115), the Major Research Project of Xiamen (3502Z20191015), the Science and Technology Service Network Initiative from the Chinese Academy of Sciences (STS2023T3039), and the Regional Key R&D Planning of Fujian Province (2021H4008).

Notes and references

1 N. A. Kukhta and M. R. Bryce, *Mater. Horiz.*, 2021, **8**, 33.
2 H. Uoyama, K. Goushi, K. Shizu, H. Nomura and C. Adachi, *Nature*, 2012, **492**, 234.
3 M. Urban, P. H. Marek-Urban, K. Durka, S. Lulinski, P. Pander and A. P. Monkman, *Angew. Chem., Int. Ed.*, 2023, **62**, e202217530.
4 M. Yang, I. S. Park and T. Yasuda, *J. Am. Chem. Soc.*, 2020, **142**, 19468.
5 C. Li, K. Zhang, Y. Luo, Y. Yang, Y. Huang, M. Jia, Y. He, Y. Lei, J. Tang, Y. Huang and Z. Lu, *Chem. Sci.*, 2024, **15**, 4790.
6 P. Wei, X. Zhang, J. Liu, G. G. Shan, H. Zhang, J. Qi, W. Zhao, H. H. Y. Sung, I. D. Williams, J. W. Y. Lam and B. Z. Tang, *Angew. Chem., Int. Ed.*, 2019, **59**, 9293.
7 M. Park, H. S. Kim, H. Yoon, J. Kim, S. Lee, S. Yoo and S. Jeon, *Adv. Mater.*, 2020, **32**, e2000936.
8 X.-H. Wu, Z. Wei, B.-J. Yan, R.-W. Huang, Y.-Y. Liu, K. Li, S.-Q. Zang and T. C. W. Mak, *CCS Chem.*, 2019, **1**, 553.
9 Q. C. Peng, Y. B. Si, Z. Y. Wang, S. H. Dai, Q. S. Chen, K. Li and S. Q. Zang, *ACS Cent. Sci.*, 2023, **9**, 1419.
10 I. Bhattacharjee, N. Acharya, H. Bhatia and D. Ray, *J. Phys. Chem. Lett.*, 2018, **9**, 2733.
11 J. Chu, Y. Oh, A. Sens, N. Ataie, H. Dana, J. J. Macklin, T. Laviv, E. S. Welf, K. M. Dean, F. Zhang, B. B. Kim, C. T. Tang, M. Hu, M. A. Baird, M. W. Davidson, M. A. Kay, R. Fiolka, R. Yasuda, D. S. Kim, H.-L. Ng and M. Z. Lin, *Nat. Biotechnol.*, 2016, **34**, 760.
12 T. Song, H. Liu, J. Ren and Z. Wang, *Adv. Opt. Mater.*, 2023, **12**, 2301215.
13 P. Li, Q. Lv, C. Sun, P. Zhang, X. Wang, C. Yin, Y. Pan and R. Chen, *J. Phys. Chem. Lett.*, 2024, **15**, 9787.
14 S. B. K. Schmidt, V. Coropceanu, D. Beljonne, J. Cornil, C. Bazzini, T. Caronna, R. Tubino, F. Meinardi, Z. Shuai and J. L. Bredas, *J. Phys. Chem. A*, 2007, **111**, 10490.
15 D. Liang, J. H. Jia, M. Yang, X. B. Cai, R. Yu and C. Z. Lu, *Adv. Opt. Mater.*, 2022, **10**, 2201130.
16 H. Nakanotani, Y. Tsuchiya and C. Adachi, *Chem. Lett.*, 2021, **50**, 938.
17 Y. Im, M. Kim, Y. J. Cho, J.-A. Seo, K. S. Yook and J. Y. Lee, *Chem. Mater.*, 2017, **29**, 1946.
18 A. Farokhi, S. Lipinski, L. M. Cavinato, H. Shahroosvand, B. Pashaei, S. Karimi, S. Bellani, F. Bonaccorso and R. D. Costa, *Chem. Soc. Rev.*, 2025, **54**, 266.
19 H. Y. Zhou, D. W. Zhang, M. Li and C. F. Chen, *Angew. Chem., Int. Ed.*, 2022, **61**, e202117872.
20 P. Rajamalli, N. Senthilkumar, P. Y. Huang, C. C. Ren-Wu, H. W. Lin and C. H. Cheng, *J. Am. Chem. Soc.*, 2017, **139**, 10948.
21 H. Takeda, A. Kobayashi and K. Tsuge, *Coord. Chem. Rev.*, 2022, **470**, 214700.
22 V. Ferraro, C. Bizzarri and S. Bräse, *Adv. Sci.*, 2024, **11**, 2404866.
23 P. Keerthika and R. K. Konidena, *Adv. Opt. Mater.*, 2023, **11**, 2301732.
24 X. Cai and S.-J. Su, *Adv. Funct. Mater.*, 2018, **28**, 1802558.
25 S. Li, L. Fu, X. Xiao, H. Geng, Q. Liao, Y. Liao and H. Fu, *Angew. Chem., Int. Ed.*, 2021, **60**, 18059.
26 L. Zhan, Z. Chen, S. Gong, Y. Xiang, F. Ni, X. Zeng, G. Xie and C. Yang, *Angew. Chem., Int. Ed.*, 2019, **58**, 17651.
27 M. Stanitska, D. Volyniuk, B. Minaev, H. Agren and J. V. Grazulevicius, *J. Mater. Chem. C*, 2024, **12**, 2662.
28 X. Yang, G. I. N. Waterhouse, S. Lu and J. Yu, *Chem. Soc. Rev.*, 2023, **52**, 8005.
29 W. Dai, Y. Jiang, Y. Lei, X. Huang, P. Sun, J. Shi, B. Tong, D. Yan, Z. Cai and Y. Dong, *Chem. Sci.*, 2024, **15**, 4222.
30 L. Li, D. Liu, J. Zhou, M. Qi, G. Yin and T. Chen, *Mater. Horiz.*, 2024, **11**, 5895.
31 C. W. Hsu, C. C. Lin, M. W. Chung, Y. Chi, G. H. Lee, P. T. Chou, C. H. Chang and P. Y. Chen, *J. Am. Chem. Soc.*, 2011, **133**, 12085.
32 R. Hamze, S. Shi, S. C. Kapper, D. S. Muthiah Ravinson, L. Estergreen, M. C. Jung, A. C. Tadle, R. Haiges, P. I. Djurovich, J. L. Peltier, R. Jazzar, G. Bertrand, S. E. Bradforth and M. E. Thompson, *J. Am. Chem. Soc.*, 2019, **141**, 8616.
33 T.-Y. Li, S.-J. Zheng, P. I. Djurovich and M. E. Thompson, *Chem. Rev.*, 2024, **124**, 4332.
34 M. Klein, N. Rau, M. Wende, J. Sundermeyer, G. Cheng, C.-M. Che, A. Schinabeck and H. Yersin, *Chem. Mater.*, 2020, **32**, 10365.
35 X. B. Cai, D. Liang, M. Yang, X. Y. Wu, C. Z. Lu and R. Yu, *Chem. Commun.*, 2022, **58**, 8970.
36 M. Z. Shafikov, R. Czerwieniec and H. Yersin, *Dalton Trans.*, 2019, **48**, 2802.
37 H. Yersin, R. Czerwieniec, M. Z. Shafikov and A. F. Suleymanova, *Chemphyschem*, 2017, **18**, 3508.
38 A. Ying, N. Li, X. Chen, J. Xia, C. Yang and S. Gong, *Chem. Sci.*, 2025, **16**, 784.
39 J.-H. Jia, D. Liang, R. Yu, X.-L. Chen, L. Meng, J.-F. Chang, J.-Z. Liao, M. Yang, X.-N. Li and C.-Z. Lu, *Chem. Mater.*, 2019, **32**, 620.
40 D. Liang, J.-H. Jia, X.-B. Cai, Y.-Q. Zhao, Z.-Q. Wang and C.-Z. Lu, *Inorg. Chem. Front.*, 2022, **9**, 6561.
41 M. Louis, H. Thomas, M. Gmelch, A. Haft, F. Fries and S. Reineke, *Adv. Mater.*, 2019, **31**, e1807887.
42 X. Wang, Y. Sun, G. Wang, J. Li, X. Li and K. Zhang, *Angew. Chem., Int. Ed.*, 2021, **60**, 17138.
43 G. Wang, X. Chen, Y. Zeng, X. Li, X. Wang and K. Zhang, *J. Am. Chem. Soc.*, 2024, **146**, 24871.
44 Y. Pan, J. Li, X. Wang, Y. Sun, J. Li, B. Wang and K. Zhang, *Adv. Funct. Mater.*, 2021, **32**, 2110207.
45 F. Neese, *Wiley Interdiscip. Rev.:Comput. Mol. Sci.*, 2022, **12**, e1606.
46 M. A. El-Sayed, *J. Chem. Phys.*, 1963, **38**, 2834.